Salt impregnated desiccant matrices for 'open' thermochemical energy conversion and storage – Improving energy density utilisation through hygrodynamic & thermodynamic reactor design.

Sean P Casey[a], Devrim Aydin[b*], Jon Elvins[c], & Saffa Riffat[d]

[a] University Centre, North Lindsey College, Kingsway, Scunthorpe, DN17 1AJ, UK

[b] Department of Mechanical Engineering, Eastern Mediterranean University, G. Magosa, TRNC Mersin 10, Turkey

[c] SPECIFIC, Baglan Energy Park, Baglan, Port Talbot, SA12 7AX, UK

[d] Division of Infrastructure, Geomatics and Architecture, Faculty of Engineering, University of Nottingham, University Park, Nottingham, NG7 2RD, UK

*corresponding author - Email: devrim.aydin@emu.edu.tr; Tel: 0090 392 630 1045

Abstract

In this study, the performance of three nano-composite energy storage absorbents; Vermiculite-$CaCl_2$ (SIM-3a), Vermiculite-$CaCl_2$-$LiNO_3$ (SIM-3f), and the desiccant Zeolite 13X were experimentally investigated for suitability to domestic scale thermal energy storage. A novel 3kWh open thermochemical reactor consisting of new meshed tube air diffusers was built to experimentally examine performance. The results were compared to those obtained using a previously developed flatbed experimental reactor.

SIM-3a has the best cyclic behaviour and thermal performance. It was found that 0,01 m^3 of SIM-3a can provide an average temperature lift of room air, ΔT = 20 °C over 180 minutes whereas for SIM-3f, ΔT < 15 °C was achieved. Zeolite provided high sorption heat in close approximation with SIM-3a, however, the higher desorption temperature requirements coupled with poor cyclic ability remain as obstacles to the roll out this material commercially.

The study results clearly show that the concept of using perforated tubes embedded inside the heat storage material significantly improves performance by enhancing the contact surface area between air → absorbent whilst increasing vapour diffusion. The results suggest a linear correlation between thermal performance and moisture uptake, ΔT – Δw. Determining these

operating lines will prove useful for predicting achievable temperature lift and also for effective design and control of thermochemical heat storage systems.

Keywords:

Salt In Matrix; Open Thermal Energy Storage; Vermiculite; Hygrothermal, Thermochemical

Nomenclature

c_p	specific heat at constant pressure	J/(kg.K)
c	temperature gradient	^oC/min
d	diameter	mm
E_d	energy density	kJ/kg, kWh/m^3
E_{cum}	cumulative thermal energy	Wh, kWh
Ex	exergy	W, kW
Ex_{cum}	cumulative thermal exergy	Wh, kWh
H	Enthalpy	kJ/s
m	mass	g, kg
m_a	mass flow rate of air	kg/s
Q	thermal power	W, kW
RH	relative humidity	%
P_v	partial vapour pressure	mbar
S	entropy	kJ/kg
t_{dwell}	time interval to reach ambient temperature	hr
t	time	s, hr
T	temperature	^oC, K
V	volume	m^3
w	absolute humidity	g/kg
ρ	density	kg/m^3
f	mass uptake ratio	g_{wv}/g_{abs}
Δ	difference	---
η_I	1st law efficiency	---
η_{II}	2nd law efficiency	---

Subscripts

tr	transferred
dr	discharging
cr	charging
g	gain
cum	cumulative
abs	absorbent
a	air

wv	water vapour
w	wet
in	inlet
out	outlet
d	dry
avg	average
f	fan
h	heating
rxn	reaction
max	maximum
g	gain

1. Introduction

Energy technologies and management strategies have been gaining more attention in the last decade as energy is vital for a safer and sustainable future. Dependency on secure energy is much higher than in the past due to growth in the industrial sector, increasing population as well as comfort demands. According to Berners-Lee & Clarke, 2013, if global warming is not to exceed 2 $^{\circ}$C then only 20 % of the worlds established fossil fuel reserves can be burned by 2050 then this energy dependency represents a major threat to the future of all humans [1]. At the current rate of fossil consumption however, it is predicted that this 2 ^{o}C rise will be achieved by the year 2030 [1].

In the built environment, the domestic building sector currently represents the highest energy consumption as more people around the world aspire to better comfort living standards, driving the demand for air conditioning and thus electrical energy [2]. Urgent energy management solutions are required to increase the share of renewable sources for this comfort energy thus reducing the over reliance on fossil fuel driven systems [3]. Within this context, various international agreements such as the Kyoto Protocol seek to address this problem [4]. In addition, the EU commission aims to increase the share of renewables to 20 % by 2020 in member countries [5, 6]. The IEO 2007 report states that domestic buildings are responsible for 40% primary energy consumption, 70% of electricity consumption and 40% of atmospheric emissions in developed countries [7, 8]. Additionally heating, cooling and air conditioning (HVAC) and domestic hot water (DWC) constitute more than half of the energy consumption in buildings [9].

Solar energy is counted as one of the primary renewable energy sources and it has promising potential for thermal applications (both space & water heating) in the domestic building sector. However, the mismatch between solar availability and building heat demand constitutes a major obstacle in residential applications usually resulting in the need for auxiliary systems / energy

sources such as heat pumps, electrical resistance heaters or gas heaters coupled with ever more sophisticated energy management systems. Although the combination of multiple systems (*i.e.* hybrid systems) enables higher energy utilisation, it also increases the complexity, capital and operational costs of these systems [10]. Heat storage systems can considerably improve the utility of solar thermal systems by acting as a 'thermal battery' by either thermo-physically or thermo-chemically storing energy for later usage. Thermophysical systems are based on either sensible heat storage (SHS) or latent heat storage (LHS) whilst thermochemical systems are based on thermochemical heat storage (THS) [11]. All these systems can allow for conversion of solar energy for either short or long term storage, dependant on system type and material used. Although both SHS and LHS systems have been widely researched in the past [12] and are somewhat mature technologies, THS is a relatively new technology for converting and storing heat with much research ongoing on these systems. Caliskan et al. [13] performed energetic, exergetic and sustainability assessments for SHS, LHS and THS. Researchers found the effectivness of three different storage methods was in the order of SHS>THS>LHS in terms of energetic and exergetic efficiency. However the main drawback of SHS compared with other storage methods is the low E_d. THS materials are gaining attention over the last decade due to their high theoretical E_d and long term heat storage potential. In this context, Henninger et al. [14] reviewed new materials for adsorptive heat transformation and storage. Similarly, Aristov [15] investigated the current trends in dynamic optimization of adsorption heat storage. An overview on sorption materials and technologies for heat pumps and thermal energy storage applications was presented by Cabeza et al. [16]. In a recent study, Scapino et al. [17] investigated the latest advancements at material and prototype scale for long term sorption heat storage. A literature survey on adsorption thermal energy storage processes for heating applications was presented by Lefebvre and Tezel [18]. Schreiber et al. [19] experimentally investigated a Zeolite based adsorption heat storage and demonstrated that heat losses have a major impact on adsorption heat storage performance, particularly in long term applications.

Gaeini et al. [20] developed a model for predicting the thermal dynamics of a Zeolite based adsorption bed concluding that the this could be useful for design and optimization of THS systems. Michel et al. [21] developed a large scale sorption reactor consisting of multiple sorption beds and air flow channels using Strontium bromide / water ($SrBr_2$ / H_2O) as a reactive pair. A novel "revolving drum" reactor prototype was investigated by Zettl et al. [22]. Likewise, a composite sorption reactor consisting of $CaCl_2$ impregnated mesoporous ceramic (Wakkanai siliceous shale) honeycomb filter was developed by Liu et al. [23] for low-temperature (< 100 °C) industrial waste heat recovery. Zhang et al. [24] experimentally investigated the performance of a 10 kWh absorption thermal energy storage prototype using LiBr–H2O. Energy storage densities for cooling, hot water and heating were found 42, 88 and 110 kWh/m^3. Lele et al, [25] investigated a closed THS system operating with $SrBr_2.6H_2O$, as an addition to cogeneration systems for storing process waste heat with a theoretical reactor E_d of 115 kWh/m^3, storage capacity of 61 kWh and thermal efficiency of 78%. In another study, Jiang et al [26] developed and experimented a sorption energy store for industrial heat recovery applications. The E_d was found in the range of 596-662 kJ/kg where energy and exergy efficiencies varied between 27.5-40.6% and 32.5-47%, respectively. Hamdan et al. [27] performed a parametric study on the potential of storing thermal energy with thermochemical heat pump using water - sodium chloride as sorbate - sorbent couple. Fernandes et al. [28] developed a dynamic model for investigating an adsorption heat storage unit (using silica gel/water pair) integrated with a solar water heating system. The results revealed that adsorption heat storage provides up to 16% savings in annual backup energy when compared with a similar conventional storage system. In a recent study, a novel sorption heat pipe that utilizes composite sorbent-sorbate (NaBr-NH_3) as working media was developed by Yu et al. [29]. In another experimental study performed by Tatsidjodoung et al. [30], it was found that an open sorption reactor loaded with 40 kg of zeolite can supply a constant power of 2.25 kW over two hours corresponding to 27.5 W kg^{-1} of material. Abedin and Rosen [31] investigated both closed and

open THS systems using energy and exergy analysis methods to evaluate the charging behavior and overall cycle performance. Balasubramanian et al. [32] developed a mathematical model to investigate the capability of salt hydrates to store thermochemical energy during their dissociation into anhydrous salts and water with an external heat supply. Researchers reported that the heat supplied for desorption is gradually absorbed by the anhydrous salt and results in an increase of desorption duration with an associated increase of heat loss to the environment. Li et al. [33] developed a composite block by impregnating BaCl inside the graphite powder pores for thermochemical conversion and storage of solar energy. In another experimental study, Mette et al. [34] developed a highly efficient regeneration process for a THS system. A zeolite based composite material was used as the absorbent. Stitou et al. [35] carried out an experimental investigation of a solar assisted THS system used for air conditioning in a pilot plant for housing in France. Tanguy et al. [36] conducted a parametric study to evaluate the impact of both the internal (air flow rate, heat exchanger pressure drop) and external conditions (outdoor temperature) on the performance of a THS system. A prototype THS system is developed by Zondag et al. [37] at the Energy Research Centre of The Netherlands. It is a packed bed sorption system which contains 0.017 m^3 of sorption material ($MgCl_2.H_2O$). They reported that an effective storage density of 0.5 GJ/m^3 was obtained from the system.

Previous studies on an 'open' THS system (*i.e.* using the building air as the heat transfer fluid with no heat exchanger) were carried out by the authors and identified three candidate materials with promising application to 'open' THS (SIM-3a, SIM-3f and Zeolite 13X). Feasibility and applicability of open THS under different climate conditions were theoretically investigated through technical, economic and environmental analyses [38-39]. A modular open sorption pipe was also developed and tested by the authors for seasonal solar energy storage [40]. It was found that system has a total energy storage capacity of 25.5 kWh and energy storage density of 290 kWh/m^3. In another study, a custom designed test rig (Gen2) was developed to assess the hygrothermal cyclic behaviour of both adsorption and thermochemical materials [41]

A new design THS system (Gen3) using perforated tubes to increase vapour diffusion to the Salt-In-Matrix (SIM) composite absorbent material was developed with the experimental results of the first phase of testing presented in this paper. The aim of this research was to improve overall energy output using the same materials tested previously, through comparative analysis of the results achieved in both rigs and further analysis of system operating parameters and the cyclic / hysteretic performance of the Gen3 rig. There are currently a very limited number of experimental studies investigating 'open' THS systems suitable for domestic building thermal energy provision in the existing literature and it is envisaged that this new concept may act as a model for future short/long term development of these systems.

2. Methodology

In previous work by the authors a range of candidate porous materials and salts capable of producing adequate exothermic thermochemical reactions for 'open' THS when hydrated were selected from the literature. From these, a total of eight SIM composites were synthesised using the Insipient Witness Technique (IWT) method [42]. These were SIM-2a, SIM-3a, SIM-3b, SIM-3c, SIM-3d, SIM-3e, SIM-4a and SIM-8a. The technique utilises a dry porous materials natural liquid absorption capacity (*i.e.* capillarity) to fill the pore structure with a desired salt solution. Whilst Vermiculite has a small level of potential sorption energy due to its high specific surface area, in this case it is used strictly as a host matrix in the composite material inhibiting deliquescence of the salt and preventing any salt leakage during the THS cycling operations. Analysis of the energy density, E_d of the materials suggested that SIM-3b (Vermiculite with $MgSO_4$) had the highest E_d of all samples however as it has very limited absorption potential this energy may not be available under standard working conditions. SIM-3a (Vermiculite with $CaCl_2$) appeared to have excellent E_d coupled with good moisture uptake and response time to moisture with TGA (Thermo gravimetric analysis) also suggesting significant mass loss in the working range $30 < T < 140$ ºC. These findings suggested that SIM-3a appears to have very good potential for use in an 'open' THS system.

From hygrothermal cycling experiments carried out using the Gen2 rig [41], Zeolite 13X provided the highest temperature lift of all samples in the first cycle due to the high amount of vapour adsorption and fast reaction kinetics. Whilst the hysteretic performance of SIM-3a was minimal, Zeolite 13X showed a sharp drop from cycle one to cycle four. Zeolite 13X requires a high regeneration temperature (> 180 ºC) with the lower regeneration temperature prerequisite for this research unable to provide adequate dehydration, however as it is used extensively in the literature it was decided to use it for comparative analysis for this work.

A new composite THS material SIM-3f was developed that combined SIM-3a and SIM-3d (Vermiculite with $CaCl_2$ and $LiNO_3$). In previous findings [42] SIM-3d was considered to be of interest as it performed well across four charge/discharge cycles albeit with a maximum temperature lift, $T_{out,\,max}$ much lower than SIM-3a which, on its own, would be too low to suit an 'open' THS system. SIM-3d appeared to have a near horizontal slope during the cyclic test (*i.e.* from maximum temperature to ambient, $T_{out,\,max} \rightarrow T_{ambient}$) suggesting that the dwell time, t_{dwell} (*i.e.* time taken for $T_{out} = T_{ambient}$) for SIM-3d may far exceed those of the other synthesised materials. It was proposed that combination of SIM-3d with SIM-3a may prove beneficial and therefore is also investigated here.

SIM-3f was prepared using equal volumes of saturated solution (50% - 50%) of each salt in separate containers to prepare the final mixed $CaCl_2$-$LiNO_3$ solution before impregnation. The solubility of $CaCl_2$ and $LiNO_3$ at room temperature (20 °C) are 745 g/l and 522 gr/l with the molar weight at the same conditions being 110.98 g/mol and 68.95 g/mol respectively. Therefore the mass ratio of $CaCl_2$ / $LiNO_3$ impregnated to the host matrix (vermiculite) was calculated as 1.42 whereas molar ratio was 0.88.

Obtained Scanning Electron Microscopy (SEM) images of raw vermiculite, SIM-3a, SIM-3f and Zeolite 13X are presented in Figure 1. Vermiculite has a micro-scale lamellar structure, enabling salt impregnation inside the voids between lamellas (See: Figure 1A). In Figure 1B,

solid crystals of $CaCl_2$ are clearly visual between the lamellas, whereas the $LiNO_3$-$CaCl_2$ mixture was coalesced within the lamellas acting more like a coating (See: Figure 1C).

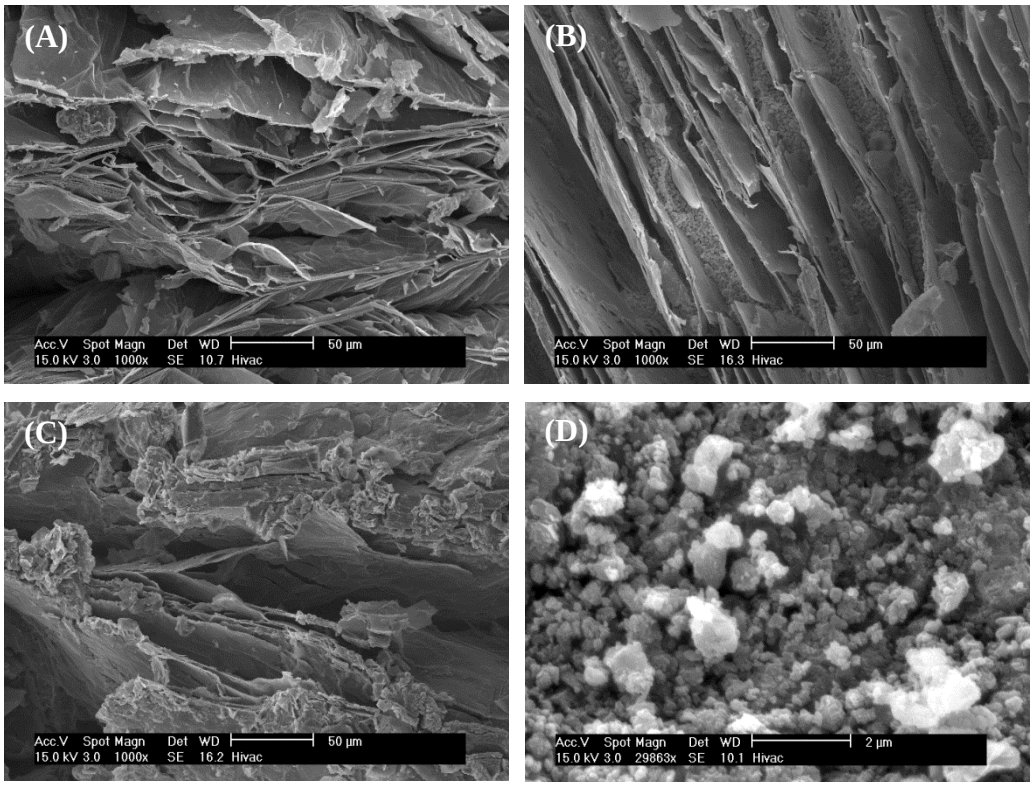

Figure 1 – SEM images of (A) raw vermiculite, (B) SIM-3a, (C) SIM-3f and (D) Zeolite 13X

Zeolite 13X has much smaller pores when compared with SIMs and as can be seen in Figure 1D, despite the use of much higher magnification ratio, the pores are not visualized. This is an advantageous aspect, enhancing the contact area between air and sorption surface in comparison with SIMs. However, smaller pore size could possibly bring a difficulty in removing the adsorbed moisture when recharging the Zeolite 13X. This could lead to higher regeneration temperatures, T_{reg}, which is an undesired situation in sorption heat storage processes.

The Gen2 testing rig (see: Figure 2-A) used in the previous research had a flat absorbent bed where the SIM material was placed on a perforated tray and air flow was perpendicular to the perforated surface. In this system there was no additional configuration allowed for to improve diffusivity and mass transfer, as the primary aim of the testing rig was to carry out a comparative performance analysis of a large number of SIM's over a short period of time. Numerical

modelling simulations on Ansys Software of the Gen2 rig showed that high resistance occurs at the reaction front which both increases the pressure drop across the absorbent bed and reduces the diffusivity and thus moisture transfer, particularly when there is an increase in SIM layer depth. This served to limit scaling-up the THS system using the Gen2 rig design.

A new testing rig (*i.e.* Gen 3), was designed and developed to demonstrate the concept/design for large scale THS applications. This system (see: Figure 2-B) was designed to investigate the hygrodynamic and thermodynamic performance of the system when using perforated tubes to facilitate vapour diffusion to the SIM to reduce the effect of the reaction front. Compared to the Gen2 rig, the Gen3 reaction chamber (8) is rectangular shaped (500 mm x 250 mm x 200 mm) with a sloping roof to facilitate post absorbent airflow and is constructed of aluminium with welded seams. Ten perforated tubes, d = 20mm, made up of 0.55 mm thick perforated aluminium sheet were placed vertically inside the reactor in two parallel rows with a horizontal distance, d = 100 mm between each (x and z direction). The tubes are connected to an external manifold (12) to equalise airflow to each tube, with the top end of the tubes sealed in order to achieve sufficient internal pressure, providing air flow laterally to the absorbent (9). Use of perforated tubes embedded inside the sorbent enhances to contact area of air and sorbent, provides uniform vapour diffusion and heat/mass transfer. In a flatbed reactor (Gen2), the vapour uptake at the reaction front is higher than the rest of the sorbent in the bed. The reaction front wets in a short period of time, blocking air flow, reducing heat output and increasing pressure drop. To overcome these issues, the Gen3 reactor was proposed as an improved design to enhance the thermal performance of THS process.

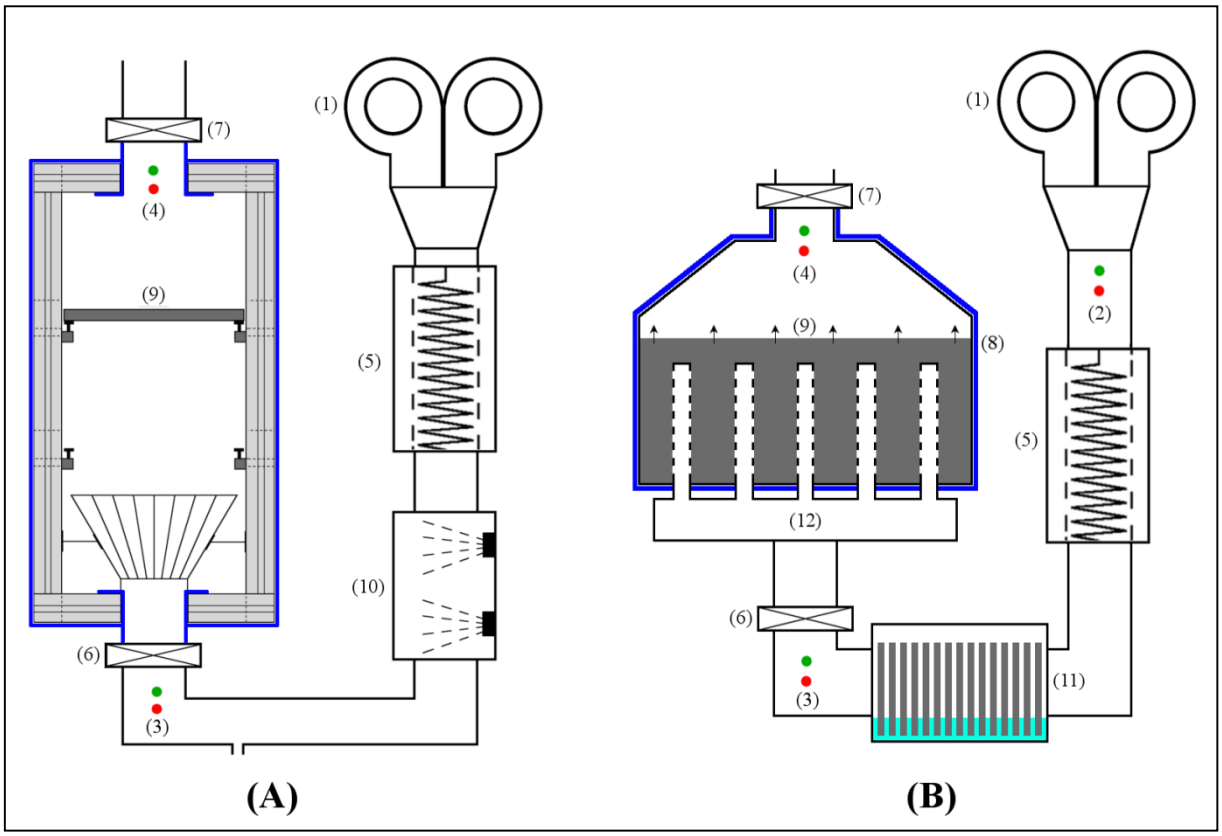

Figure 2 – Schematic diagram of (A) the Gen2 and (B) the Gen3 experimental test rigs.

Humidification of the inlet air is provided using an evaporative pad matrix placed inside a rectangular shaped wick chamber (11). Air flow through the wick chamber is parallel to the evaporative pads, enabling moisture enhancement of the inlet air before entering the reaction chamber. An Xpleair (UK) XID series, inline duct fan (1) (d = 150 mm) is used to provide air flow and is connected to ducting (d = 100 mm) via a reducer. To eliminate thermal losses to the external environment, the complete system is insulated using 25 mm thick, foil lined glass wool. Temperature and relative humidity (RH) were recorded using the EK-H4 Eval Kit for Temperature - Humidity Sensors from Sensiron, AG, Switzerland. Three sensor locations were used – (2) ambient, (3) manifold inlet and (4) reactor outlet.

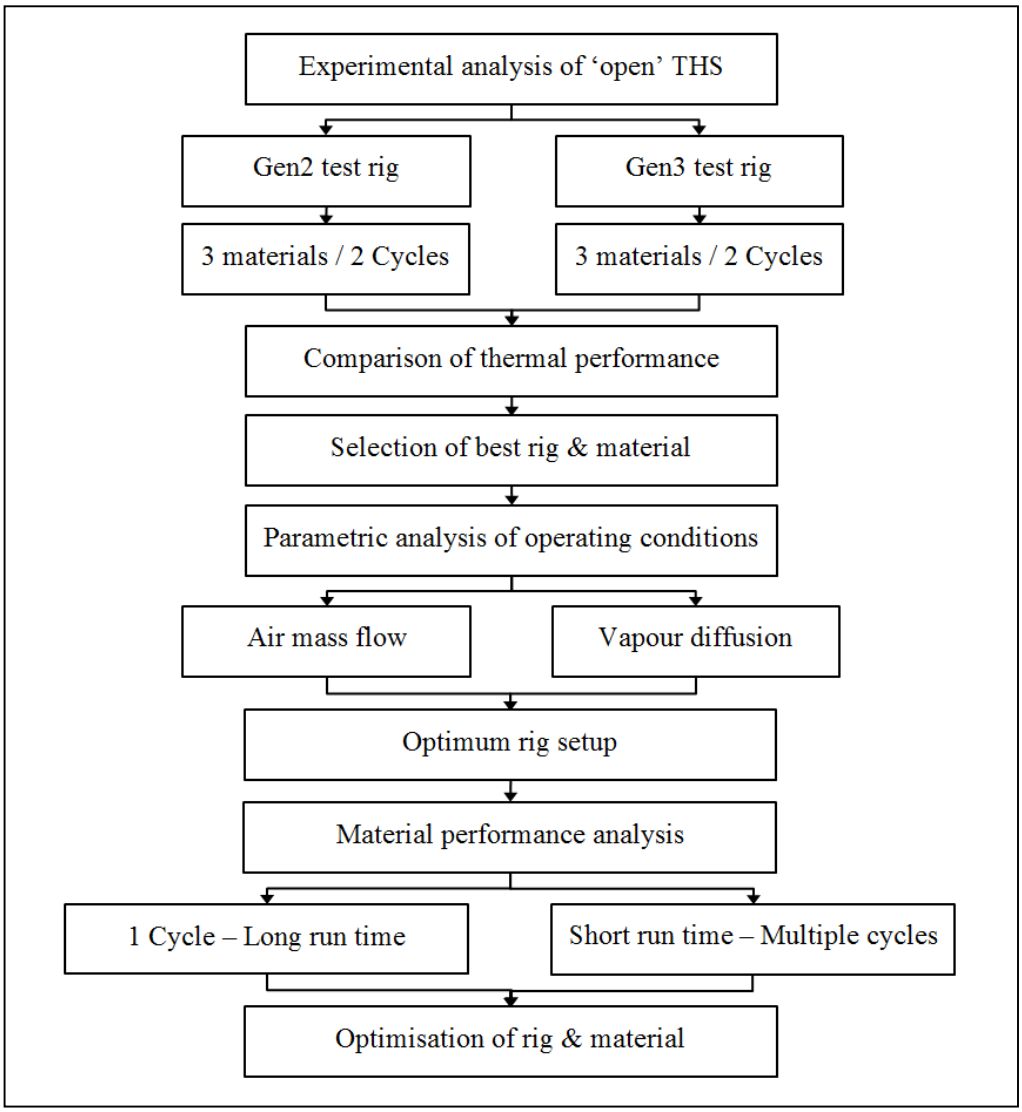

Figure 3 – Graphical flow chart of the experimental methodology.

The experimental methodology was divided into two phases (see: Figure 3). The first phase included a comparative energetic, exergetic and hygrothermal analysis of the three selected materials' performance in the Gen2 and newly developed Gen3 rigs. In the second phase, the best performing material from the first phase would be selected for parametric analysis using the Gen3 rig. This analysis would chart the effect on performance (*i.e.* temperature lift and moisture uptake) of i) tube hole diameter and ii) air flow rate. Additionally, both the long and short term cyclic behaviour of the SIM material with correlations between mass change, Δw and temperature change, ΔT were investigated.

3. Comparison of performance between Gen2 and Gen3

In this section an analysis of both the energetic and exergetic experimental results collected during the testing period is presented and discussed with the formulas used in the analysis given in Table 1a-c. All samples were prepared by oven drying at $T \approx 150$ ºC for a period, t >24 h to achieve the condition $m_{dry} = 0$ kg/kg. The dry SIM was then placed in a mesh tray and allowed to cool in a desiccator for $t = 2$ h prior to testing. When cooled, the material was placed into the reaction chamber and the rig sealed. During the charging of the materials, partial vapour pressures (P_v) for SIM-3a and SIM-3f were varied in the range of 764 →0 mbar and 853→0 mbar indicating that both SIMs were fully regenerated at 150 ºC. On the other hand, P_v for Zeolite 13X dropped from 582 to 82 mbar and then remained constant demonstrating that Zeolite 13X requires higher temperatures for fully desorption to occur. As the aim was to test material performance under identical operating conditions, no further desorption at higher temperatures were applied to Zeolite 13X. As a result, its performance sharply dropped over repeating discharging cycles, whereas performance of the SIM's were much steadier as discussed in detail in the following sections of the paper.

For the discharging cycle (absorption), the humidifier was connected and the psychrometric state of the airflow monitored. When the desired humidity level was reached, the inlet valve was opened. Each test was carried out over two short discharging cycles of duration $t_{cycle} = 180$ min each with charging of the material occurring between each cycle. For the charging cycle (desorption) the humidifier was disconnected and the heating unit activated and set to the desired regeneration temperature ($T = 90$ ºC). The charging cycle was deemed to be complete when;

$$RH_{out} = RH_{in} \quad \text{or} \quad \Delta m \leq 2\% \quad \text{or} \quad T_{in} = T_{out}$$

Definition	Unit	Equation	Equation No.
Instantaneous heat gain	kW	$\dot{Q}_g = \dot{H}_{out,dr} - \dot{H}_{in,dr}$	1a
		$\dot{Q}_g = \dot{m}_{dr}.c_p.\left(T_{out,dr} - T_{in,dr}\right)$	1b
Energy density	Wh/g	$E_d = \frac{E_{cum,dr}}{\Delta m_{ads}}$	2
	kWh/m^3	$E_{d,dr} = \frac{E_{cum,dr}}{V_{ads}}$	3
Mass increase	g	$\Delta m_{dr} = M_{wv} = M_w - M_d$	4
Mass uptake ratio	---	$f_{dr} = \frac{M_{ads,x} - M_{ads,d}}{M_{ads,d}}$	5
Absolute humidity	g/kg	$w = 216.7.\left[\frac{\frac{RH}{100\%}.6.112.exp\left(\frac{17.62.T}{243.12+T}\right)}{273.15+T}\right]$	6
Cumulative thermal energy generation	kWh	$E_{cum} = \dot{m}_{dr}.c_p.\int_0^{t_d}\left(T_{out,dr} - T_{in,dr}\right)dt$	6
Exergy gain	kW	$\dot{E}x_g = (\dot{E}x_{out,dr} - \dot{E}x_{in,dr})$	7a
		$\dot{E}x_g = \dot{m}_{dr}.[(h_{out,dr} - h_{in,dr}) - T_a.(s_{out,dr} - s_{in.dr})]$	7b
		$\dot{E}x_g = \dot{m}_{dr}.c_p.[(T_{out,dr} - T_{in,dr}) - T_a.\ln\left(\frac{T_{out,dr}}{T_{in,dr}}\right)]$	7c
COP	---	$COP_{dr} = \frac{\dot{Q}_{g,avg}}{\dot{W}_f}$	8

Table 1a- Equations for analysis of the discharging process

	Unit	Equation	Equation No.
Instantaneous heat transfer to absorbent	kW	$\dot{Q}_{tr} = \dot{H}_{in,cr} - \dot{H}_{out,cr}$	9a
		$\dot{Q}_{tr} = \dot{m}_{cr}.c_p.\left(T_{in,cr} - T_{out,cr}\right)$	9b

Cumulative energy transfer to absorbent	kWh	$E_{cum,c} = \dot{m}_{cr}.c_p.\int_0^{t_c}(T_{in,cr} - T_{out,cr})dt$	10
Desorption heat transfer	Wh/g	$E_{d,cr} = \frac{E_{cum,cr}}{\Delta m}$	11
Removed moisture	g	$\Delta m_{cr} = M_{wv} = M_w - M_d$	12
Mass release ratio	---	$f_{cr} = \frac{M_{ads,w} - M_{ads,x}}{M_{ads,w}}$	13
Exergy transfer to absorbent	kW	$\dot{Ex}_{tr} = (\dot{Ex}_{in,cr} - \dot{Ex}_{out,cr})$	14a
		$\dot{Ex}_{tr} = \dot{m}_{cr}.[(h_{in,cr} - h_{out,cr}) - T_a.(s_{in,cr} - s_{out,cr})]$	14b
		$\dot{Ex}_{tr} = \dot{m}_{cr}.c_p.[(T_{in,cr} - T_{out,cr}) - T_a.\ln\left(\frac{T_{in,cr}}{T_{out,cr}}\right)]$	14c
Charging efficiency	%	$\eta_{cr} = \frac{\dot{Q}_{tr}}{\dot{W}_f + \dot{Q}_h}$	15

Table 1b - Equations for analysis of the charging process

Definition	Unit	Equation	Equation No.
1st law efficiency	---	$\eta_{I,rxn} = \frac{\dot{Q}_{g,ave}}{\dot{Q}_{tr,ave}}$	16
2nd law efficiency	---	$\eta_{II,rxn} = \frac{\dot{Ex}_{g,ave}}{\dot{Ex}_{tr,ave}}$	17

Table 1c - Equations for analysis of system efficiencies

The P_v of the outlet air during the charging cycles of SIM-3a, SIM-3f and Zeolite 13X were in the range of 375→21 and 416→14 and 310→63 mbar respectively. Some residual moisture remained in all materials at T_{reg} = 90 ºC (the moisture content was highest in Zeolite 13X and lowest in SIM-3f after desorption).

In Figure 4, the discharging inlet and outlet temperatures, T_{in} and T_{out}, of SIM 3a, SIM-3f and Zeolite 13X tested in both the Gen2 and Gen3 rigs are presented with the full data set from test and subsequent analysis summarized in Table 2. The purpose of these tests was to compare the Gen2 and Gen3 testing rigs and demonstrate any performance improvement. In THS systems, contrarily to both SHS and LHS systems, effective mass transfer (moisture) is required, which can significantly reduce performance as the size of the THS system increases. If we assume that the heat storage capacity of all these systems is directly proportional to the amount of material employed, then novel designs which provide efficient moisture diffusion are therefore required to enable efficient sorption processes in larger storage units.

An 'open' THS system operation is based on the temperature lift of a building's air due to the energy conversion associated with moisture absorption. Due to the thermochemical reaction, there is a sharp temperature lift of output air at the beginning of the reaction and, as time passes, the moisture content inside the reactor increases and moisture sorption rate of THS material (*i.e.* sorption kinetics) slows down causing a drop in temperature. For thermal analysis of the tests, four measures are used here:

1. Maximum output temperature, $T_{out,\,max}$, which is the peak temperature reached in each single cycle
2. End state temperature lift, ΔT_{180}, which represents the temperature lift at the end of the cycle *i.e.* $T_{out} - T_{in}$ @ t = 180 min
3. Dynamic output temperature drop, c, which is the gradient from $T_{out,\,max}$, to $T_{out,\,180}$, ($\mathrm{d}T/\mathrm{d}t$)
4. Average temperature lift, ΔT_{avg}, which is the average temperature differential over the full cycle i.e. $T_{out} - T_{in}$ / 180

The results show that the performance of all three materials increased across all four measures when using the Gen3 testing rig as opposed to the Gen2 rig.

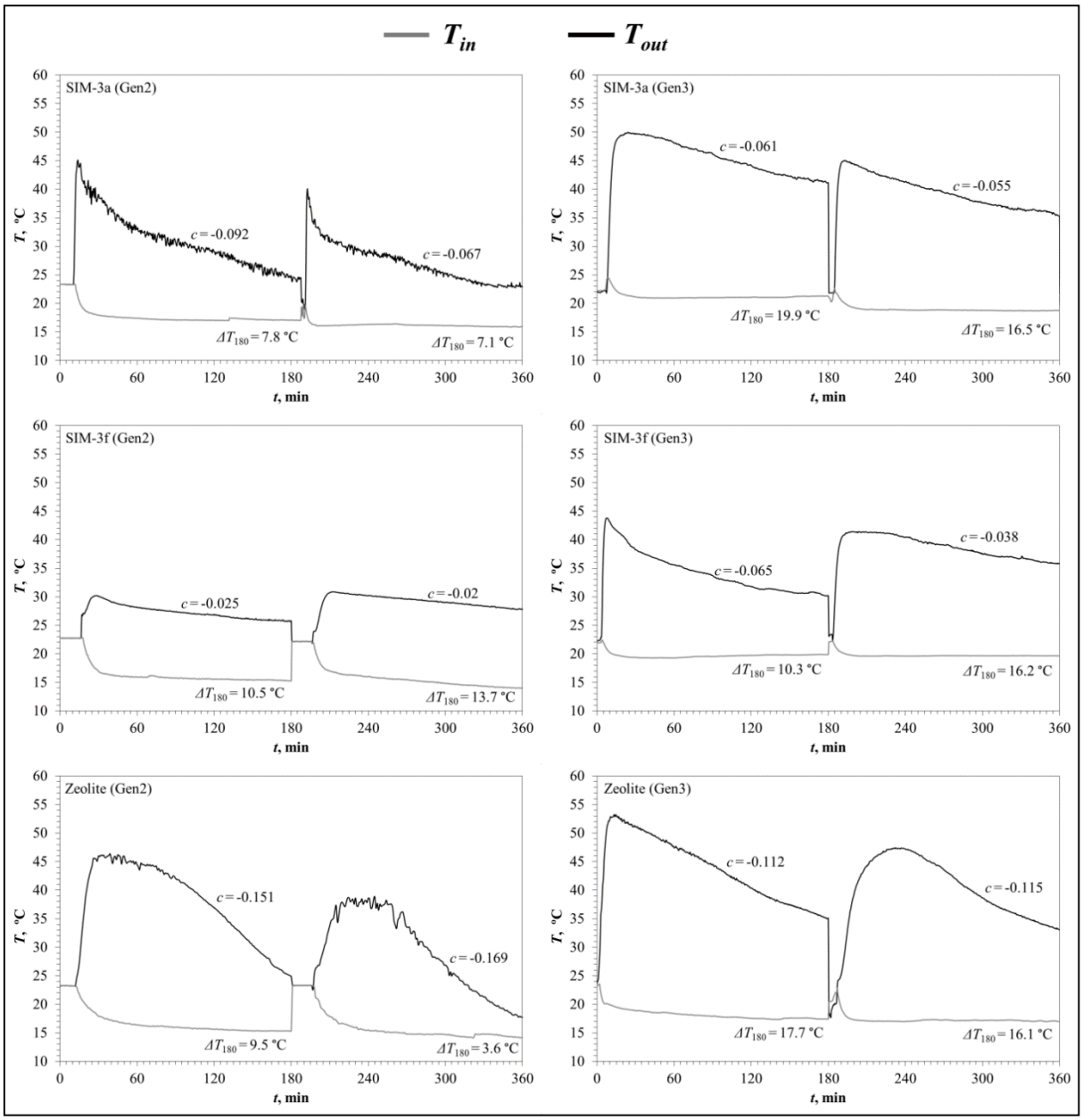

Figure 4 – Three hour limited generation cycles for SIM-3a, SIM-3f and Zeolite 13X using the Gen2 and Gen3 experimental rigs.

To ease notation in the text, the first cycle of each test is denoted as $^{(1)}$ whilst the second cycle is noted as $^{(2)}$. The results for SIM-3a (Vermiculite/$CaCl_2$) clearly indicate the significant improvement in Gen3 rig with an average temperature lift ΔT_{avg} = 23 °C$^{(1)}$ and 19.9 °C$^{(2)}$ compared with 12.8 °C$^{(1)}$ and 10.7 °C$^{(2)}$ in Gen2. In both cycles of the Gen2 rig, a sharp drop in outlet temperature, T_{out} was observed with dynamic output temperature drops of, c = 0.092$^{(1)}$ and 0.067$^{(2)}$ for the Gen2 rig compared with 0.061$^{(1)}$ and 0.055$^{(2)}$ for Gen3 which are shallower and indicate better performance due to the increased diffusion and steadier vapour absorption of SIM-3a in Gen3 after the wetting of the reaction front. Initial maximum temperatures are

also higher in Gen3 with, $T_{out,\,max}$ = 50 ºC$^{(1)}$ and 45 ºC$^{(2)}$ as opposed to 45 ºC$^{(1)}$ and 40 ºC$^{(2)}$. Although there was only a 5 ºC difference observed in $T_{out,\,max}$ it is the end state temperature difference that indicates the superior performance of Gen3 over Gen2 with ΔT_{180} values of 19.9 ºC$^{(1)}$ and 16.5 ºC$^{(2)}$ in Gen3 against 7.8 ºC$^{(1)}$ and 7.1 ºC$^{(2)}$ in Gen2.

For SIM-3f (Vermiculite/$CaCl_2$/$LiNO_3$) both the average and peak temperature lift was higher in Gen 3. Although the temperature lifting of SIM-3f was poor in Gen2, it showed a steadier performance across both cycles with gradients c = 0.025$^{(1)}$ - 0.020$^{(2)}$ in Gen2 and 0.065$^{(1)}$ - 0.038$^{(2)}$ in Gen3. End state temperature difference, ΔT_{180} for cycle 1 was similar in Gen2 and Gen3, however, in cycle two, Gen3 was considerably higher, ΔT_{180} = 16.2 °C than 13.7 °C in Gen2. Average temperature lift was also higher for Gen 3, ΔT_{avg} = 14.3°C$^{(1)}$ and 18.5°C$^{(2)}$ as opposed to Gen 2 with ΔT_{avg} = 10.2 °C$^{(1)}$ and 12.4 °C$^{(2)}$ indicating improved performance.

Zeolite 13X's performance was also significantly enhanced using the perforated tubes (Gen3) in comparison to Gen2. A sharp drop was observed in both cycles for the Gen 2 rig with ΔT_{180} = 9.5 °C$^{(1)}$ and 3.6 °C$^{(2)}$ representing a falloff in performance of 5.9 °C between the cycles. In Gen 3 however, performance is much steadier with ΔT_{180} = 17.7 °C$^{(1)}$ and 16.1°C$^{(2)}$ representing a small drop of 1.6 ºC between cycles. The improved performance in Gen 3 was due to the uniform air flow and better diffusivity through the material. This condition is evidenced with the comparison of the ΔRH_{avg} (see: Table 2) achieved in Gen 2 and Gen 3 and demonstrates three facts;

1. Reducing ΔRH_{avg} (32.5 %$^{(1)}$ → 24.4 %$^{(2)}$) between cycles led to a notable performance drop of Zeolite 13X (ΔT_{ave} 20 °C$^{(1)}$ → 12.5 °C$^{(2)}$) in the Gen2 testing rig. This was an expected outcome, as the change in P_v across the material is directly related with sorption heat generation. However, despite the targeted drop (per 1% change) in ΔRH_{avg} being < 0.5 °C, experimental results showed that the drop is ~1 °C.
2. Steady ΔRH_{avg} (75.3%$^{(1)}$ → 75.7%$^{(2)}$) provided a more stable performance without any significant drop in the Gen3 testing rig.

3. The higher ΔRH_{avg} in Gen3 enabled higher average temperatures, ΔT_{avg} = 5.2 °C$^{(1)}$ and 9.5 °C$^{(2)}$ with consequently higher energy density, E_d of 13.8$^{(1)}$ and 35.2$^{(2)}$ kWh/m^3.

The cyclic energetic (η_I) and exergetic (η_{II}) efficiencies of the materials in Gen2 and Gen3 are presented in Figure 5. SIM-3a provided improved η_I and η_{II} in the Gen3 rig in both cycles. $\eta_I^{(1)}$ for SIM-3a varied between 0.79→0.71 whereas $\eta_I^{(2)}$ was found to be 0.63→0.53. As a result of the exergy losses and exergy destruction, η_{II} was much lower for both test rigs. $\eta_{II}^{(1)}$ was calculated as 0.25→0.19 whilst $\eta_{II}^{(2)}$ was 0.18→0.13 in two repeating cycles. η_I for Sim-3f was similar in both test rigs. Using Gen3, η_I varied between 0.52- 0.61 for both test rigs, $\eta_{II}^{(1)}$ was 0.04 and $\eta_{II}^{(2)}$ was 0.09-0.013 in two cycle testing of SIM-3f.

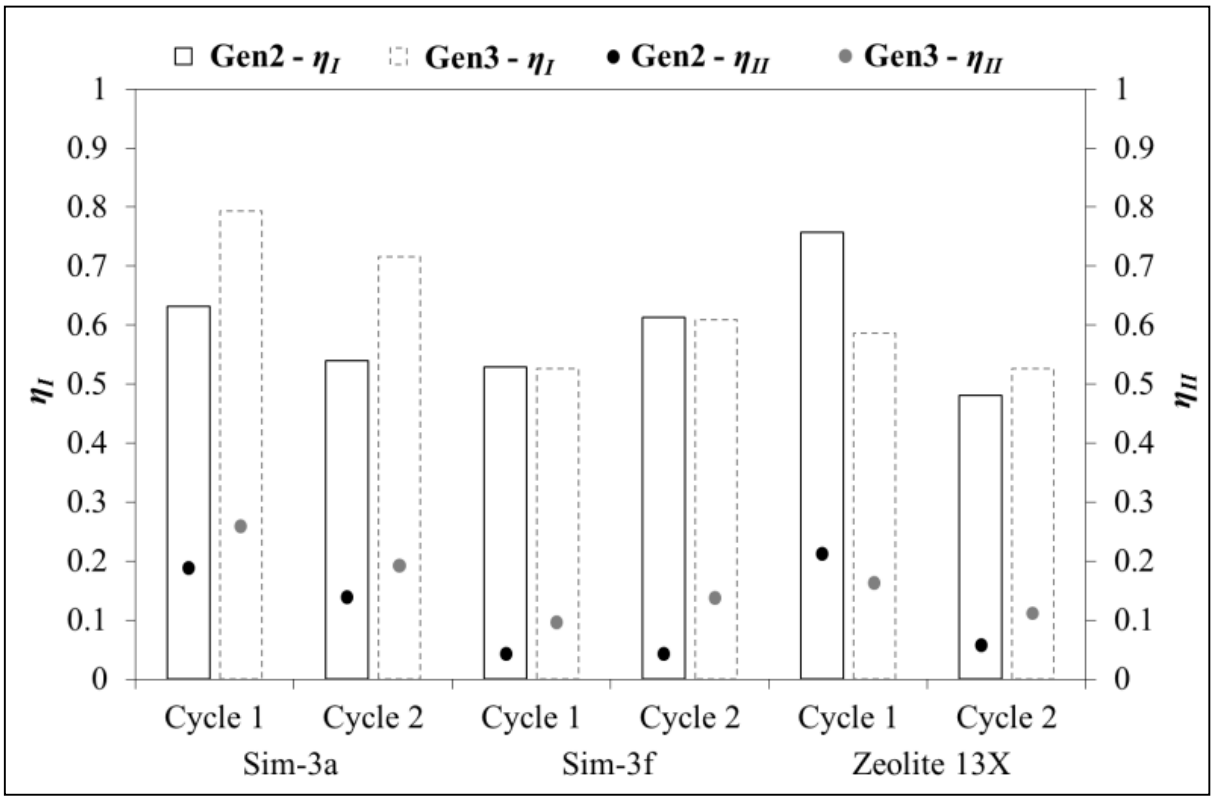

Figure 5 – Energetic and exergetic efficiency of materials in Gen2 and Gen3 testing rigs

Although the performance of Zeolite 13X in the Gen2 rig was superior, it dropped sharply in the following cycle due to the poor moisture desorption (*i.e.* regeneration). $\eta_I^{(1)}$ for the initial cycle of Zeolite 13X was 0.75 which was the highest among all performed tests. $\eta_I^{(1)}$ was found

to be only 0.48 in the repeating cycles however, which was the lowest obtained efficiency. The Zeolite 13X's performance in the Gen3 rig was found much steadier, where $\eta_I^{(2)}$ was 0.58→0.53. In terms of second law performance, $\eta_{II}^{(1)}$ dropped substantially to the range of 0.21→0.05, whereas $\eta_{II}^{(2)}$ was relatively steadier (0.16→0.11). Results indicate that SIM-3a performs best in terms of both energetic-exergetic efficiencies and also has the most promising thermal stability.

Mass uptake ratio, f_{dr}, for the discharging cycle and mass loss ratio, f_{cr}, for the charging cycle of all materials in Gen2 and Gen3 rigs are presented in Figure 6. According to previous testing results, the moisture removal ratio (MRR= $m_{ads,dr}/ m_{des,cr}$) in Gen2 rig was 0.91, 0.95 and 0.72 for SIM-3a, SIM-3f and Zeolite 13X respectively. For the Gen3 rig, MRR was found to be 0.95, 0.93 and 0.77 for the same order of materials. A low MRR indicates a drop in desorbed moisture during the charging cycle which results in a drop of adsorption energy and thus poor heat output in following discharging cycles.

This suggests that, SIM-3a and SIM-3f effectively regenerate at the applied regeneration temperature (T_{reg} = 90 °C) with an MRR > 0.9. The MRR for Zeolite 13X was < 0.8 however, explaining the reason for its poor cyclic ability and thermal stability under the same operating conditions. Theoretically, assuming a constant inlet air P_v for all materials, the corresponding T_{out} values will be in the range of $T_{out,SIM\text{-}3a} > T_{out,SIM\text{-}3f} > T_{out,Zeolite}$ due to the higher MRR and higher heat output per unit of moisture uptake of SIM's.

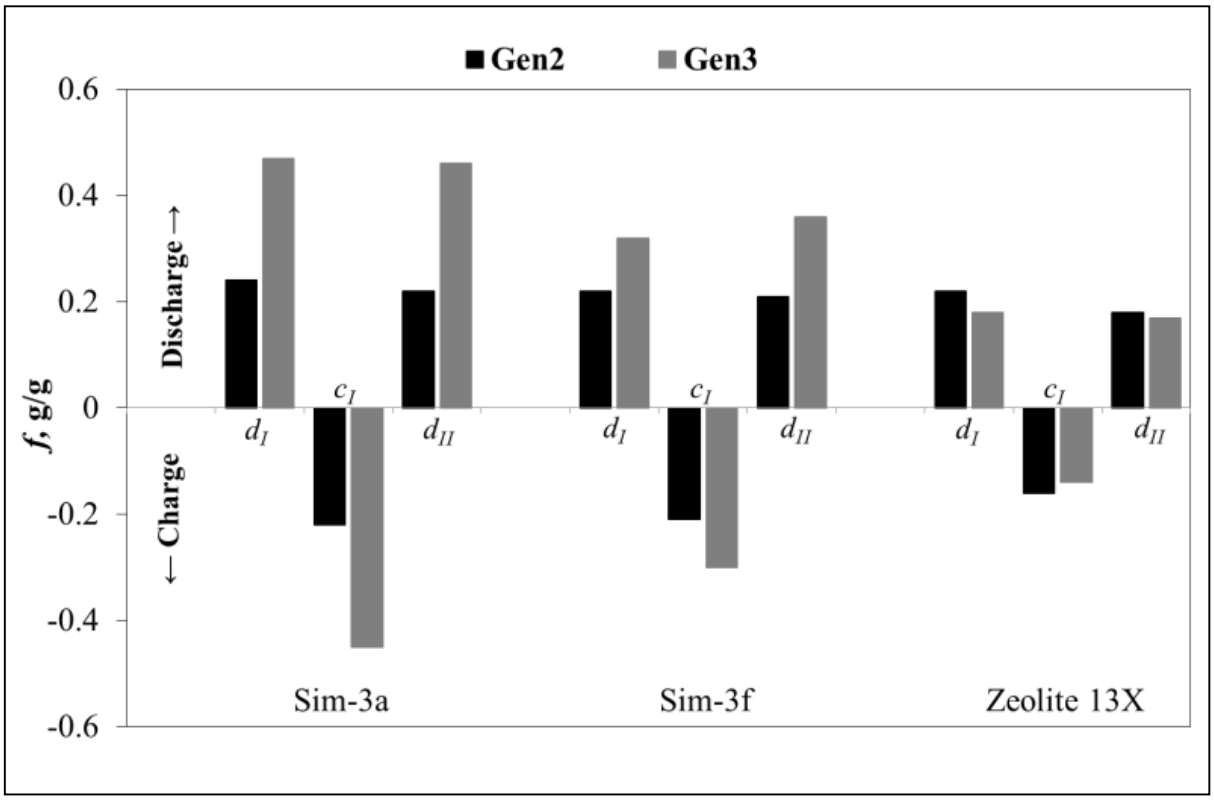

Figure 6 – Mass uptake ratio of the materials in Gen2 and Gen3 testing rigs

Two other important measures for comparing material performance in both testing rigs are E_d and COP_{dr} as presented in Figure 7. The E_d used in the analyses is the ratio of total heat output (total enthalpy change of air across the sorbent) per m^3 of the sorption material over the discharging period under a constant inlet air P_v of 20 mbar. COP_{dr} is the ratio of heat output to total electrical work input to the system during discharging. Improved E_d was obtained for SIM-3a and Zeolite 13X in Gen3 rig, whilst E_d SIM-3f was slightly higher using the Gen2 rig. Using the Gen3 rig, the $E_d^{(1)}$ and $E_d^{(2)}$ of SIM-3a was between 104→80 kWh/m^3 and 112→97 kWh/m^3 respectively. SIM-3f provided an E_d of 101 kWh/m3 in the 2nd cycle of testing in Gen2 rig, which was the second highest among all performed cycles. In contrast, the lowest E_d achieved was in the second cycle testing of Zeolite 13X in the Gen2 rig, due to the poor heat output in that discharging cycle. The summary of the obtained E_d's across all tests are presented in Table 2.

Zeolite 13X provided the highest COP_{dr} in the Gen2 rig, which was approximately 21, however a substantial drop was observed in the second cycle, similar to the other measures as presented

previously. When the COP_{dr} average across two cycle testing of materials was considered, $COP_{dr}^{(1)}$ was 12, 12, 17 for SIM-3a SIM-3f and Zeolite 13X respectively. For the same order, $COP_{dr,ave}^{(2)}$ *was* calculated as) 17, 13 and 15. Whilst the $COP_{dr,ave}^{(1)}$of both Zeolite 13X and SIM-3a were found to be equal, the steadier performance of SIM-3a over further repeating cycles would probably lead to higher COP values.

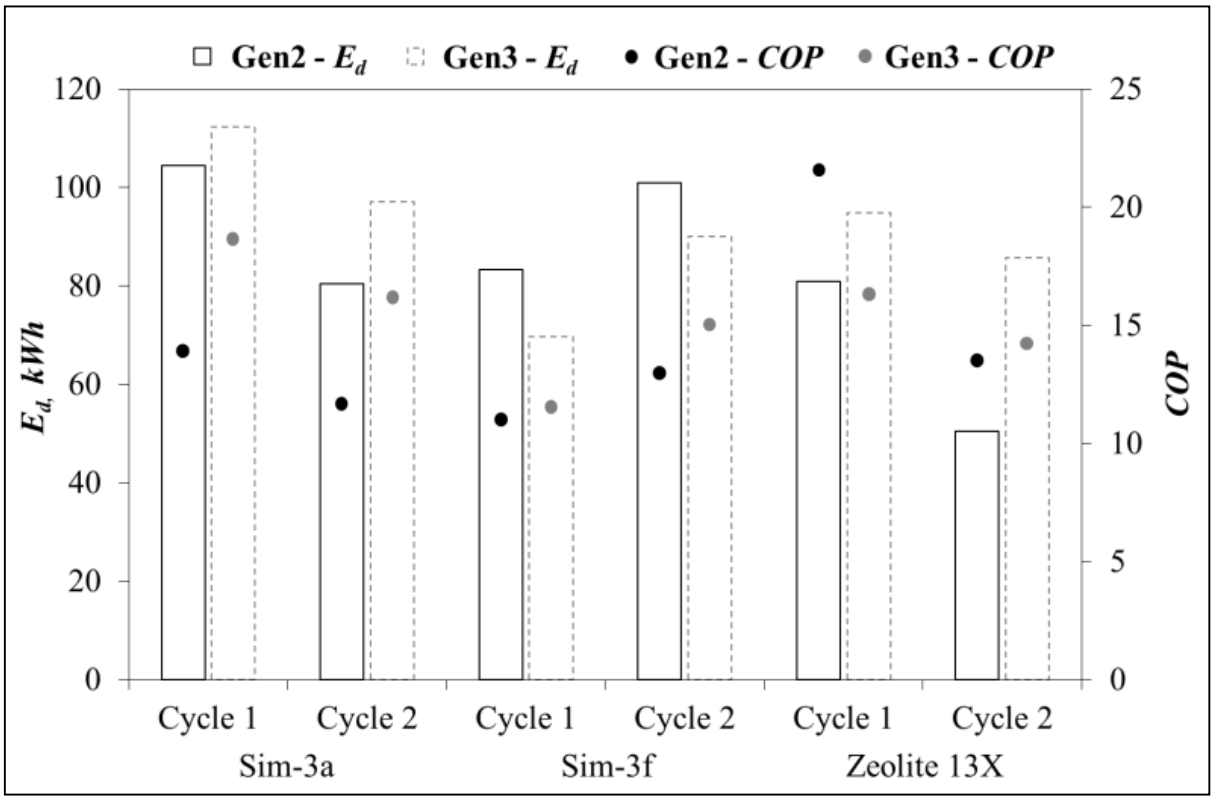

Figure 7 – Energy density and COP of the materials in Gen2 and Gen3 testing rigs

Looking holistically across all the chosen performance criteria (Q_g, Ex_g, ΔT, *MRR*, η_I, η_{II}, COP_{dr} and E_d), the most promising results were for SIM-3a in the Gen3 rig. $CaCl_2$ is highly hygroscopic and will continue to absorb moisture until deliquescence occurs. The combination of this remarkable property with its high E_d (45 kJ/mole) makes it a very promising candidate for domestic THS applications.

Whilst it was expected that SIM-3f would perform better than SIM-3a however this couldn't be achieved in the experiments. This could be due to the change in chemical structure of $LiNO_3$ and $CaCl_2$ when mixed, thereby altering the thermochemical properties of both salts. $CaCl_2$ shows a rapid response to moisture and has a high sorption rate when used individually.

Conversely, $LiNO_3$ has a slow response to moisture and low sorption rate resulting in a lower but steadier heat output. As the water attraction of $CaCl_2$ is higher, it has a higher water desorption temperature than $LiNO_3$ which is not desired. The salts were mixed to create a composite with the aim of lowering the desorption temperature and increasing the moisture sorption-desorption stability of $CaCl_2$ and, as a result, consuming less energy in charging cycles. However, $LiNO_3$ dominated the new composite and the sorption rate remained low. Furthermore there wasn't any major increase in desorption rate of SIM-3f when compared with SIM-3a indicating that the drop of regeneration temperature was not significant. All these outcomes showed that the individual use of $CaCl_2$ is more advantageous.

SIM-3a has a lower critical humidity thereby higher affinity to water vapour when compared with SIM-3f and Zeolite 13X. The uniform allocation of salt and larger pore size of SIM-3a (See: Figure 1) promotes better vapour sorption and desorption in charging and discharging cycles. Additionally, as the salt is located between the lamellas rather than randomly sticking on the vermiculite surface, redistribution of salt / pore blocking are minimised over repeating cycles. These aspects explain the better hygrothermal and cyclic performance of SIM-3a among the three tested absorbents.

Utilising $CaCl_2$ as the thermochemical media and vermiculite as the host matrix constitutes a spectacular composite absorption material for conversion and storage of solar energy or waste heat.

	Test rig	Cycle No	ΔRH (%)		ΔT (°C)		f (g_{wv}/g_{abs})	E_{cum} (Wh)	Ex_{cum} (Wh)	Q (W)		Ex (W)		E_d	
			Peak	Avg.	Peak	Avg.				Peak	Avg.	Peak	Avg.	kWh/m^3	Wh/g
SIM-3a	Gen 2	1	47.9	27.6	24.6	12.8	0.24	209	3.4	133.3	69.5	4.7	1.1	104.5	1.61
		2	47.3	27.6	22.7	10.7	0.22	161	2.1	120.2	58.3	3.1	0.7	80.5	1.40
	Gen 3	1	76.1	66.7	28.6	23.0	0.47	1123	35.1	464.1	373.1	17.6	11.6	112.3	0.67
		2	83.5	71.7	25.3	19.9	0.46	971	24.8	410	323.6	14.2	8.2	97.1	0.59
SIM-3f	Gen 2	1	39.2	29.5	13.3	10.2	0.22	166	0.6	71	55	0.7	0.2	83.3	1.26
		2	30.8	23.9	14.3	12.4	0.21	202	0.8	77	65	0.7	0.2	101	1.64
	Gen 3	1	65.2	50.3	23.0	14.3	0.32	697	10.3	374.8	231.8	11.5	3.4	69.7	0.77
		2	65.9	61.2	21.7	18.5	0.36	901	19.1	352.6	300.5	8.7	6.3	90.1	0.66
Zeolite 13X	Gen 2	1	52.9	32.5	29.2	20	0.22	162	4.0	157.6	108.2	5.5	2.6	81.0	0.65
		2	46.2	24.4	23.4	12.5	0.18	101	1.1	124.7	67.8	2.5	0.7	50.5	0.49
	Gen 3	1	94.8	75.3	33.4	25.2	0.18	948	25.8	435.9	327	17.6	8.5	94.8	0.69
		2	90.3	75.7	30.3	22.0	0.17	857	17.5	393.5	285	11.3	5.8	85.7	0.65

Table 2 - Full results data set for the Gen2 & Gen3 testing rigs material based performance comparison.

4. Parametric analysis of operating conditions

In this section the experimental results of the best performing absorbent (SIM-3a), tested in the Gen3 rig using different tube configurations and different mass flow rates are presented. The aim was to investigate the effect of the perforated tube's hole diameter (acting as an air diffuser) on heat and mass transfer. The thermal performance of SIM-3a using three different mass flow rates was also analysed to determine the optimum operational conditions.

4.1. Vapour Diffusion - tube configuration

In 'open' THS reactor design, perforated diffuser tubes can be considered crucial components and their effectiveness can determine the performance of the entire heat storage process. As in the previous section, the measures ΔT_{180}, ΔT_{avg} and $T_{out,\ max}$ are used to determine the heat storage effectiveness. In THS process, the aim is to achieve a steady temperature output (see: Figure 4) rather than a very high peak at the beginning followed by a sharp drop. Considering that building heat loads are dynamic, heat storage performance should be predictable to allow simple design and management for space heating applications. In this context perforated tubes with 1 mm (d_1), 2 mm (d_2) and 3 mm (d_3) hole diameters were tested to compare their performance and determine the most suitable size. The diameter of the holes in the air diffusers can significantly influence the thermal performance of the THS system as hole size has an impact of the pressure and velocity of the air diffusing into the sorption material. To investigate the impact of hole size on THS performance, three different perforated tubes were tested. The temperature and *RH* variation of the process air during testing is given in Figure 8 and Figure 9. It is clearly seen from Fig. 4 that d_3 provided a sharp temperature lift ($T_{out,\ max}$ >48 °C) at the beginning of the reaction followed by d_1 and d_2 with $T_{out,\ max}$ >42 °C. In terms of overall performance, ΔT_{avg} was found to be very similar for all three hole sizes (16.1 °C, 16.4 °C and 15.9 °C for d_1, d_2 and d_3 respectively).

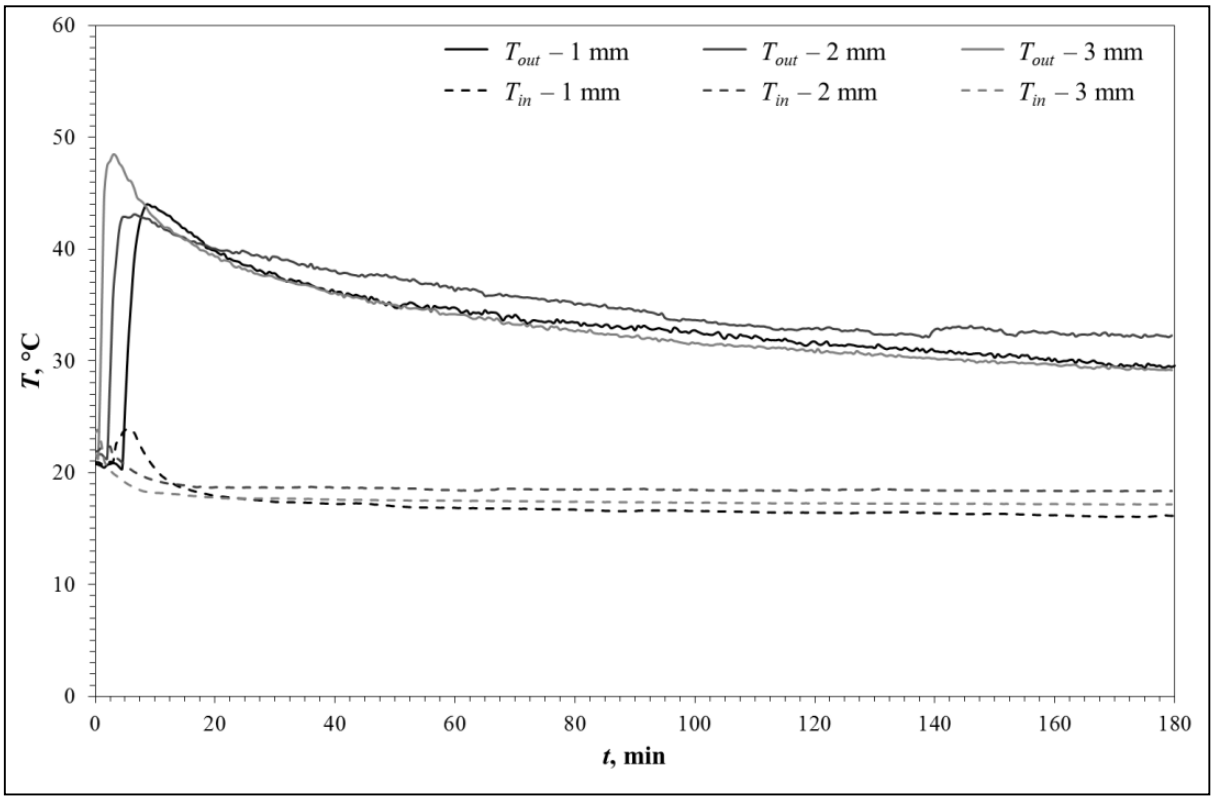

Figure 8 – Temperature variation of SIM-3a with different tube configurations in the Gen3 testing rig.

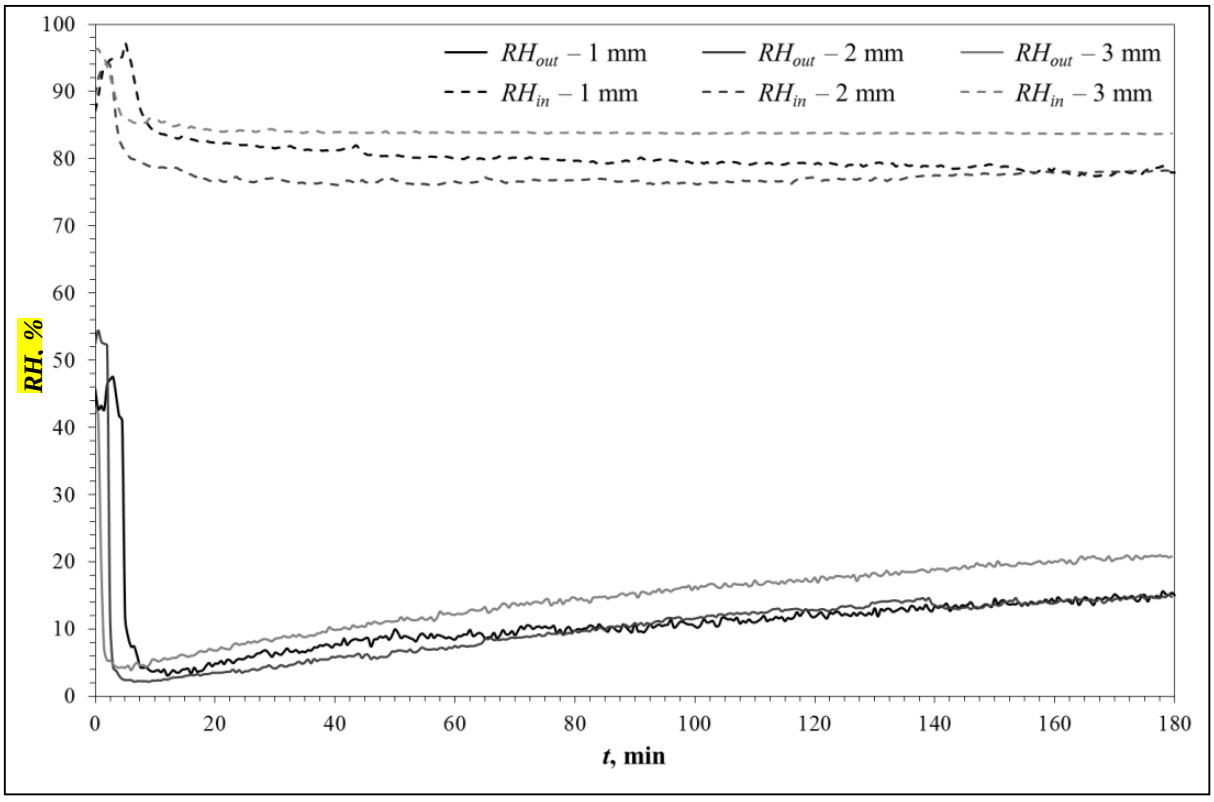

Figure 9 – Relative humidity variation of SIM-3a with different tube configurations in the Gen3 testing rig.

The cumulative energy and exergy measures, E_{cum} and Ex_{cum} confirm the greater performance of d_2 with values of 640 Wh and 12.3 Wh compared with d_1 and d_3 (630 Wh/618 Wh and 9.6 Wh/10.2 Wh respectively).

Figure 9 illustrates the RH of both inlet and outlet air for cycles with different tube configurations. As the novel evaporative humidification unit consists of evaporative pads without any additional moisture supply (e.g. water spray, atomizer, ultrasonic humidifier), a controlled amount of vapour was added to the air in each test, however there was still a slight variation to reactor inlet RH due to the varying humidity of the laboratory environment during each testing period. The higher $T_{out,\,max}$ observed for d_3 could be due to the slightly higher inlet RH where d_3 reached RH = 85% whereas d_1 and d_2 were lower at RH ≈ 77% at the end of 180 minutes. The moisture uptake ratio, f was found as 0.28, 0.29 and 0.31 g_{wv}/g_{abs} for d_3, d_1 and d_2 respectively. Whilst there is not any significant difference between the effectiveness of perforated tubes with different hole sizes, d_2 seems to be the best candidate for achieving a steadier performance over longer periods of heat storage. Therefore d_2 was selected for the remaining tests investigating the effect of mass flow rate on thermal performance, evaluating the cyclic stability and long term behaviour of SIM 3a.

4.2. Air mass flow rate

Although ‘open’ THS is a relatively simple method for heat storage, it involves a complex process of energy conversion via absorption where mass (moisture transfer from air to the adsorbent) and heat (from adsorbent to the process air) transfer is dynamic and occurs simultaneously. The mass flow rate of the inlet air has therefore a significant effect on overall heat storage performance. This includes the influence of both moisture and air which are either directly or indirectly related with achievable temperature lift, ΔT.

For instance, a high mass flow rate can provide higher heat generation as it carries more moisture to the absorbent however a higher amount of dry air is thus also required to be heated

at the same time. Simply, increasing humidity has a positive influence on ΔT while increasing the dry air volume has a negative influence. A high rate of moisture absorption (from higher RH) also creates a "wetting effect" on the absorbent which can cause sensible cooling of both the absorbent and the process air. It should also be noted that the heat storage capacity of any finite mass of sorption material is limited and a high rate of moisture sorption will lead to high initial thermal power release from the absorbent, but with low process time as the temperature lift drops sharply in a short period of time. Conversely, a low mass flow rate may lead to insufficient moisture supply to the absorbent and may not provide enough pressure for uniform air and moisture diffusion throughout the entire absorbent. This condition can lead to several undesired consequences such as low temperature lift, low reaction kinetics, non-uniform moisture sorption and moisture condensation at the reaction front. To investigate the effect of air mass flow rate on discharging output temperature, a one cycle test under three different air mass flow rates was performed.

Figure 10 illustrates the inlet and outlet air temperature for three different cycles with three air mass flow rates (0.012 kg/s, 0.015 kg/s and 0.02 kg/s). The results demonstrate considerably improved performance with the mid-range flow rate (0.015 kg/s) with $T_{out,\,max}$ = 50 ºC and ΔT_{180} = 20 °C compared to the lower (0.012 kg/s) and higher (0.02 kg/s) flow rates.

The output temperature from the reactor is a function of the air mass flow rate and vapour absorption rate of the sorbent. With an increasing air mass flow rate, the amount of air to be heated per unit time is greater. Therefore, a higher mass flow rate (0.02 kg/s) leads to a drop in T_{out}. On the other hand, a low air mass flow rate (0.01 kg/s) reduces the amount of vapour supplied to the sorbent. As a result, any absorption heat generated remains insufficient to increase the air temperature above 45 ºC. As seen in Figure 10, when a lower amount of vapour supply is used, the rate of heat generation is lower; therefore, T_{out} is much steadier at a low air mass flow rate (0.01 kg/s) compared with the higher mass flow rate. At a mid-range air mass flow rate (0.015 kg/s) ratio of the amount of air to be heated and vapour supplied to the sorbent

per unit time is optimal. This condition led to a substantial increase in T_{out} when compared with both the higher and lower air mass flow rates.

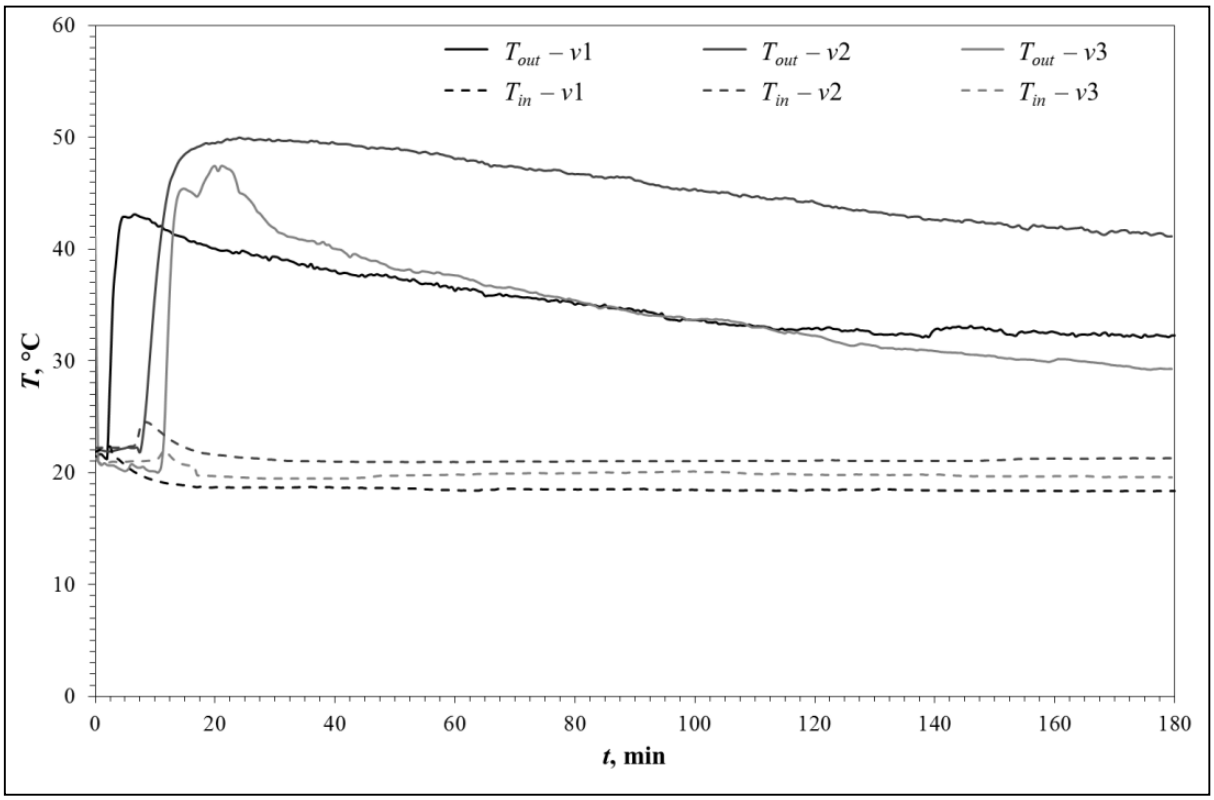

Figure 10 - Temperature variation of SIM-3a with different air mass flow rates in the Gen3 testing rig.

These results demonstrate that whilst there is not any direct correlation between THS performance and air flow rate / humidity, each reactor design will have a unique optimum flow rate which should be carefully analysed (numerically or experimentally) in order to achieve the optimum thermal output from the system.

5. Cyclic analysis of material performance

5.1. Analysis of a single long cycle

The long term performance of one cycle of SIM-3a, which provided the most promising results previously are presented in Figure 11. To investigate the maximum thermal energy that can be extracted from SIM-3a using the Gen3 testing rig, this cycle was allowed to run until the condition $T_{out} = T_{in} + 3$ °C was achieved (at the end of 20 hours for this case).

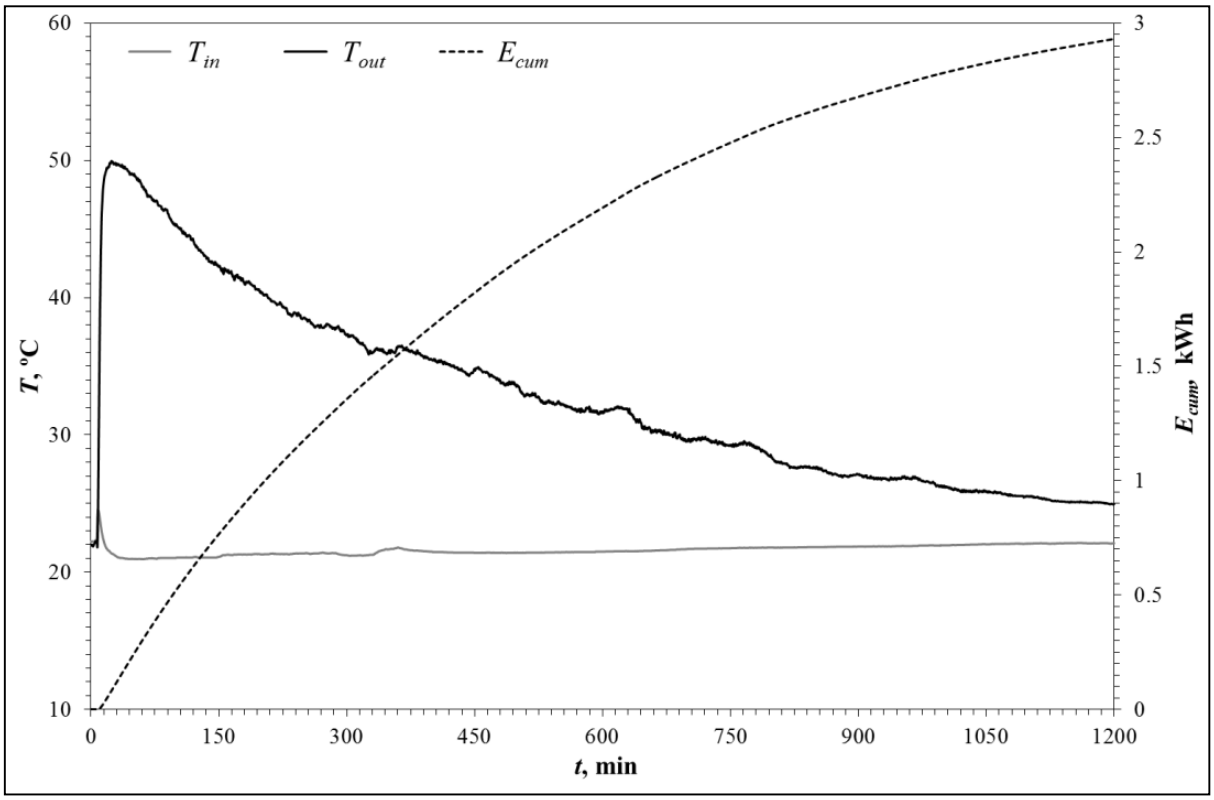

Figure 11 – Thermal performance of SIM-3a over 1200 min. testing in Gen3 testing rig

During the test period the total thermal energy output reached 2.93 kWh in comparison with the 1.12 kWh at the end of first three hours in the previous tests (see: Table 2) with mass uptake tripling to 1.41 from 0.47 g_{wv}/g_{abs}. It is interesting that 2.93 kWh was achieved using only 0.01 m^3 of storage volume, suggesting that THS has remarkable potential for reducing the space requirement for heat storage systems in future low/zero carbon buildings.

Figure 12 illustrates the correlation of Δw and ΔT over 20 hours testing of SIM 3a where Δw is the absolute humidity difference (w_{in}- w_{out}) and ΔT is the temperature difference (T_{out}- T_{in}) of inlet and outlet air during the discharging cycle. During the test period (t = 20 h), it can be observed that the correlation between Δw and ΔT is almost linear and independent of time. In theory, this would allow monitoring of performance drops as a result of reducing mass uptake trends over repeated cycles. For instance, the rate of mass uptake would decrease with the reduced inlet air partial pressure, air mass flow rate or reduced bed height in the discharging cycle. As a result, the temperature lift, ΔT, will be lower. Utilizing the correlation presented in Figure 12, would allow determining the best possible ΔT for any particular operational

condition or reactor configuration. Recognizing and using this correlation in the future should allow easier and more efficient design and management conditions for THS systems.

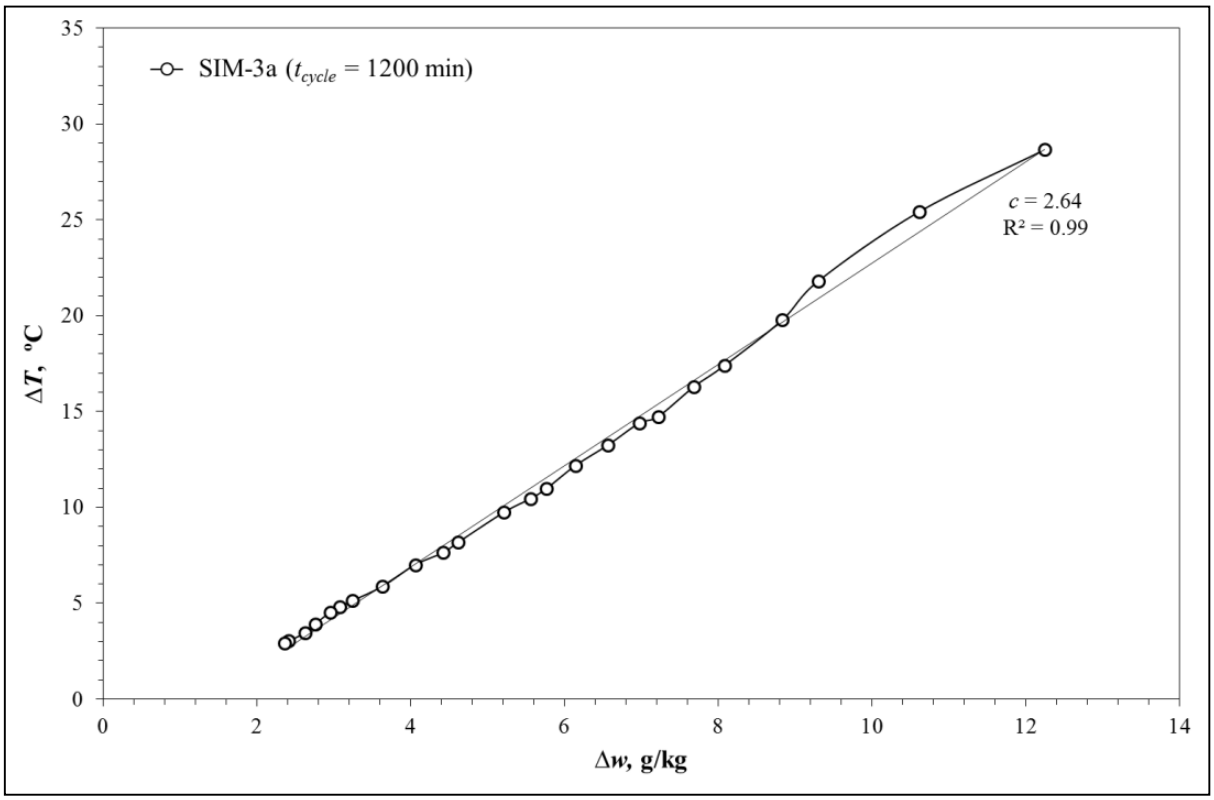

Figure 12 – Correlation between Δw and ΔT for SIM-3a in the Gen3 rig

5.2. Analysis of multiple short cycles

The last stage of testing was to analyse the cyclic behaviour of SIM-3a in order to simulate its performance for long term (cyclic) heat storage applications. Based on the previous results, an air flow rate of 0.015 m^3/s and perforated tubes with hole diameter of d = 2 mm were used during the tests. Due to technical difficulties with the rig during these cycles, SIM-3a was recharged at T = 90 °C for 24 hours following each discharging cycle in an externally located oven. For that purpose, all material was removed from the reactor and placed inside the oven in a perforated tray. As a natural convection oven was used for desorbing the moisture, charging duration was long (close to 24 hours). If charging was done in the reactor, it would be expected to be shorter due to the forced convection applied with the air flow. This would enhance the desorption rate thereby using charging heat input more efficiently.

Figure 13 represents the inlet and outlet temperatures and thermal energy output in each of the four cycles. ΔT_{180} showed a decreasing trend from the 1st cycle to 4th cycle in the order of 19.5 °C → 17.2 °C → 14.8 °C → 13.2 °C which was somewhat expected. Similarly, cumulative energy outputs, E_{cum}, were 1.12 kWh → 0.96 kWh → 0.87 kWh → 0.74 kWh with cumulative exergy outputs, Ex_{cum}, calculated as 0.035 kWh → 0.024 kWh → 0.018 kWh → 0.013 kWh in the order 1st → 4th cycle respectively.

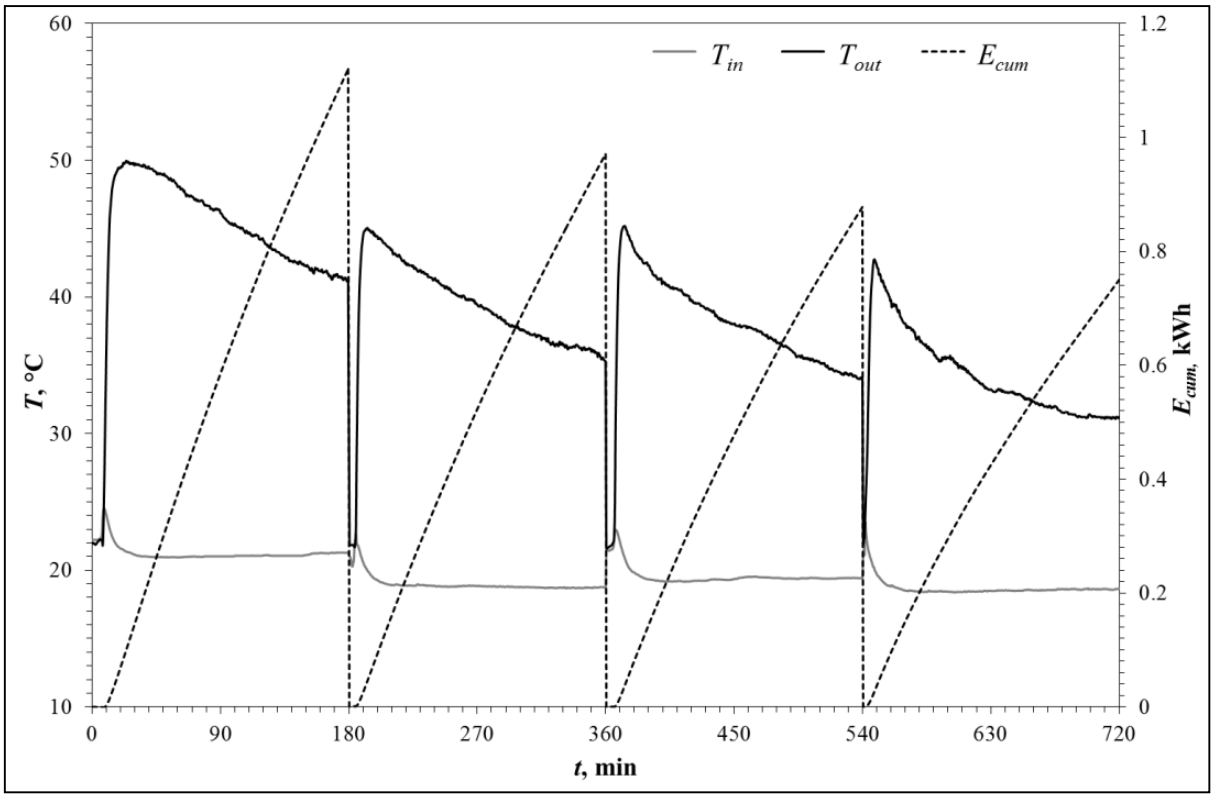

Figure 13 – Cyclic performance of SIM-3a in the Gen3 testing rig

In terms of energy output this corresponds to a performance drop of 14% for the 1st → 2nd cycle, 9% for the 2nd → 3rd cycle and 14% for the 3rd → 4th cycle. One possible reason for the performance drop could be insufficient drying of the material as an electrical oven was used for recharging the material (*i.e.* static air). Usage of a hot/dry air flow through the material could be more effective as air convection could significantly contribute to moisture removal from the material. Greater drying of the absorbent would undoubtedly achieve greater cyclic performance of SIM-3a as the material did not show any physical degradation over the cyclic testing. The performance drop is the result of the reducing trend of mass uptake over the four

repeated cycles supporting the correlation discussed earlier between moisture supplied to the material and temperature lift (See: Figure 12). This is due to the residual moisture remaining in the material at the applied T_{reg} (90 °C). If T_{reg} were increased to 120 °C, theoretically anhydrous SIM-3a would be achieved and at that condition, steady T_{out} profiles could be obtained over repeating cycles. However it should be noted that, increasing T_{reg} will significantly increase the required sorption heat and this could lead to a sharp drop in THS cyclic efficiency. Therefore, T_{reg} = 90 °C was determined as the optimal temperature for SIM-3a dehydration.

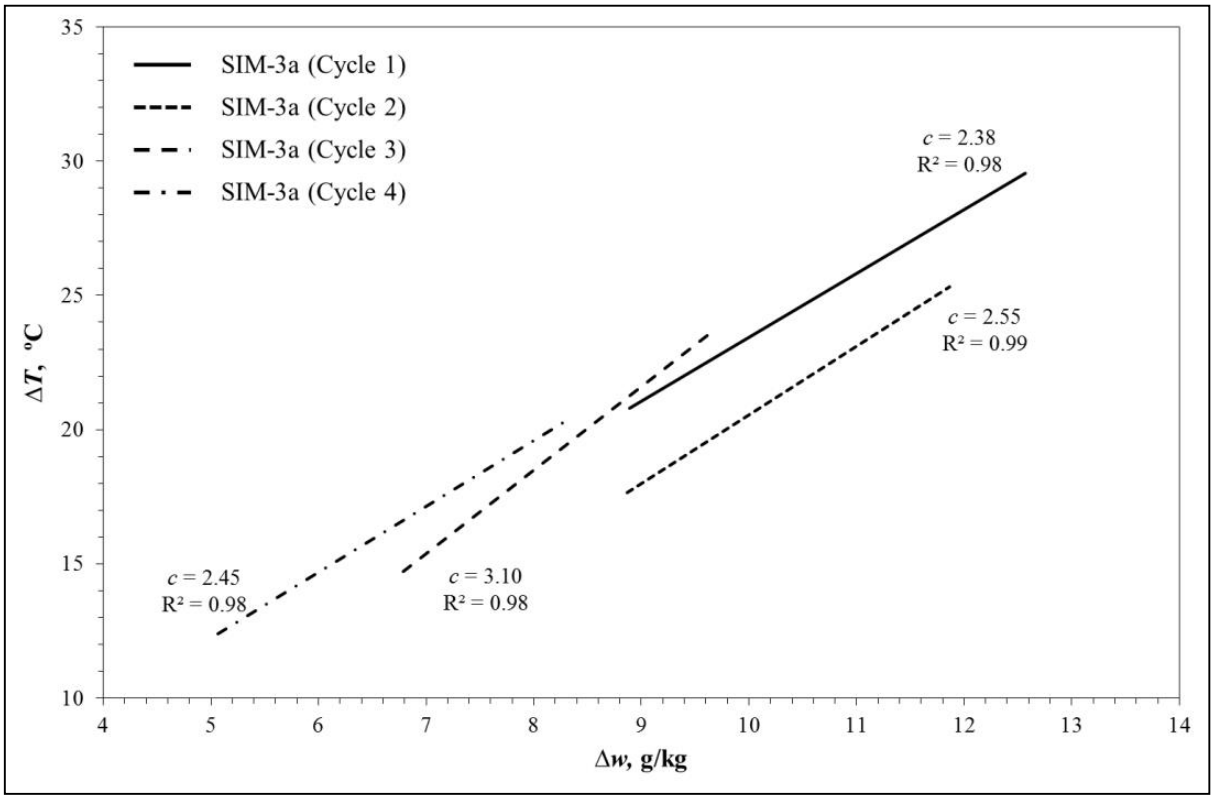

Figure 14 – Correlation between Δw and ΔT over four cycle testing of SIM-3a in Gen3 rig

As in the long cycle, Figure 14 illustrates the almost linear correlation between instantaneous Δw and ΔT for the four repeated cycles. Although there are slight differences for each cycles line however, all of them are in close approximation and can therefore be generalized to simulate THS performance according to the Δw of the process air. Obviously, it would be of benefit to have a considerable amount of repeated cycles (~20 cycles) to truly assess the cyclic performance of the process and draw a more realistic operating line, unique for a certain design/absorbent, indicating the achievable temperature lift for a specific change in Δw. In

addition it should be noted that under real UK winter climate conditions it may not be possible to supply high moisture levels to the absorbent which could lead to poor system performance. For instance an ambient temperature, T_a = 10 °C and RH_a = 50% would correspond to a w_a = 3.77 gr/kg. Under these psychrometric conditions, even if the air is saturated to 100% RH, w_a will be limited to 7.5 gr/kg. This is the maximum moisture amount that could be supplied to the absorbent and, even if all the moisture were fully absorbed, the theoretical maximum temperature lift achievable would ΔT_{peak} < 20 °C (based on the operating line proposed earlier). Therefore in real applications, especially under severe winter conditions, pre-heating the air before entering the humidifier by some solar source or recycling a certain amount of the outlet air from the heat storage reactor could significantly improve heat storage performance by increasing w_a considerably. Further studies on this concept are planned as next step of this research.

6. Conclusions

In this study the thermal performance of three different absorbents were experimentally investigated using two different testing rigs. The aim was to both compare material performance and rig design/performance. The main findings were;

- SIM-3a provided the best performance in terms of thermal performance and multi-cyclic ability. Although Zeolite also presents good thermal properties it fails due to its high regeneration temperature requirement. SIM-3a also has a lower cost and greater potential for commercial usage.
- SIM-3f unexpectedly showed relatively poor performance against the other absorbents. V-$LiNO_3$ was added to increase the performance of SIM-3a, however this was not successful.
- The Gen3 test rig provided improved performance over Gen2. The use of perforated tubes enhances both moisture and heat transfer allowing for higher and steadier temperature lift

during discharging. The tubes increase mass transfer into the absorbent, with minimal resistance, which is one of the current challenges in 'open' THS systems.

- An air mass flow rate of 0.015 kg/s was optimal as it provided the highest temperature lift.
- There is a direct and linear correlation between the amount of water vapour supplied to the absorbent and the temperature lift. This shows that low inlet air temperature limits the water vapour that can be added to the air. This is critical in winter conditions where storage is most required. Use of solar energy (if available) or circulating some of the output heat during the discharging process to preheat the incoming air would improve heat storage performance.

Acknowledgements

The authors wish to gratefully acknowledge the support of Innovate UK for funding the research presented in this paper as part of a larger project (101223 'INTRESTS'). The authors also wish to acknowledge BASF (UK & Ireland) for their assistance in procuring the materials for this research.

References

1. Berners-Lee M, Clark D. *The Burning Question: We can't burn half the world's oil, coal and gas. So how do we quit?* 2013: Profile Books.

2. Aydin D, Casey SP, Riffat S. *The latest advancements on thermochemical heat storage systems.* Renewable and Sustainable Energy Reviews 2015; **41**(0): 356-367.

3. Utlu Z, Aydin D, Kincay O. *Comprehensive thermodynamic analysis of a renewable energy sourced hybrid heating system combined with latent heat storage*. Energy Conversion and Management 2014; **84**: 311–325.

4. Zhou D, Zhao CY, Tian Y. *Review on thermal energy storage with phase change materials (PCMs) in building applications.* Applied Energy 2012; **92**: 593-605.

5. Böhringer C et al. *EU climate policy up to 2020: An economic impact assessment.* Energy Economics 2009; **31**: 295-305.

6. Böhringer C,. Rutherford TF, Tol RS. *The EU 20/20/2020 targets: An overview of the EMF22 assessment.* Energy Economics 2009; **31**: 268-273.

7. IEA *Key World Energy Statistics 2009*. 2009.

8. IEA, *International energy outlook 2007*, 2007, Energy Information Administration.

9. Parameshwaran R et al. *Sustainable thermal energy storage technologies for buildings: a review.* Renewable and Sustainable Energy Reviews 2012; **16**(5); 2394-2433.

10. Badescu V. *Model of a solar-assisted heat-pump system for space heating integrating a thermal energy storage unit.* Energy and Buildings 2002; **34**(7): 715-726.

11. Gur I, Sawyer K, and Prasher R. *Searching for a better thermal battery.* Science 2012; **335**(6075): 1454-1455.

12. Aydin D, Utlu Z, Kincay O. *Thermal performance analysis of a solar energy sourced latent heat storage*. Renewable and Sustainable Energy Reviews 2015; **50**(0): 1213-1225.

13. Caliskan H, Dincer I, Hepbasli A. *Thermodynamic analyses and assessments of various thermal energy storage systems for buildings.* Energy Convers Manage 2012; 62: 109–22.

14. Henninger S et al. *New materials for adsorption heat transformation and storage.* Renewable Energy 2016; Article in press.

15. Aristov Y. *Adsorptive transformation and storage of renewable heat: Review of current trends in adsorption dynamics.* Renewable Energy 2016; Article in Press.

16. Cabeza LF, Sole A, Barreneche C. *Review on sorption materials and technologies for heat pumps and thermal energy storage.* Renewable Energy 2016; Article in Press.

17. Scapino L et al. *Sorption heat storage for long-term low-temperature applications: A review on the advancements at material and prototype scale.* Applied Energy 2017; 190: 920–948.

18. Lefebvre D, Tezel FH. *A review of energy storage technologies with a focus on adsorption thermal energy storage processes for heating applications.* Renewable and Sustainable Energy Reviews 2017; 67: 116–125.

19. Schreiber H et al. *Heat lost or stored: Experimental analysis of adsorption thermal energy storage*. Applied Thermal Engineering 2016; 106: 981–991.

20. Gaeini M, Zondag HA, Rindt CCM. *Effect of kinetics on the thermal performance of a sorption heat storage reactor*. Applied Thermal Engineering 2016; 102: 520–531.

21. Michel B, Mazet N, Neveu P. *Experimental investigation of an innovative thermochemical process operating with a hydrate salt and moist air for thermal storage of solar energy: Global performance.* Applied Energy 2014; **129**: 177–186.

22. Zettl B, Englmair G, Steinmaurer G. *Development of a revolving drum reactor for open-sorption heat storage processes.* Applied Thermal Engineering 2014; **70**:42-49.

23. Liu H, et al. *Honeycomb filters made from mesoporous composite material for an open sorption thermal energy storage system to store low-temperature industrial waste heat.* International Journal of Heat and Mass Transfer 2013; **65**: 471–480.

24. Zhang X, Li M, Shi W, Wang B, Li X. *Experimental investigation on charging and discharging performance of absorption thermal energy storage system.* Energy Convers Manage 2014; 85: 425–34.

25. Lele AF, Kuznik F, Opel O, Ruck WKL. *Performance analysis of a thermochemical based heat storage as an addition to cogeneration systems.* Energy Conversion and Management 2015; 106: 1327–1344.

26. Jiang L et al. *Experimental investigation on an innovative resorption system for energy storage and upgrade.* Energy Conversion and Management 2017; 138:651–658.

27. Hamdan MA, Rossides SD, Khalil RH. *Thermal energy storage using thermochemical heat pump*. Energy Convers Manage 2013; 65: 721–4.

28. Fernandes MS et al. *A thermal energy storage system provided with an adsorption module – Dynamic modeling and viability study*. Energy Conversion and Management 2016; 126: 548–560

29. Yu Y et al. *The feasibility of solid sorption heat pipe for heat transfer.* Energy Conversion and Management 138; 2017:148–155.

30. Tatsidjodoung P et al. *Experimental and numerical investigations of a zeolite 13X/water reactor for solar heat storage in buildings*. Energy Conversion and Management 2016; **108**: 488–500.

31. Abedin AH and Rosen MA. *Closed and open thermochemical energy storage: Energy- and exergy-based comparisons.* Energy 2012; **41**(1): 83-92.

32. Balasubramanian G et al. *Modeling of thermochemical energy storage by salt hydrates.* International Journal of Heat and Mass Transfer, 2010; **53**(25–26): 5700-5706.

33. Li, T., et al., *Performance analysis of an integrated energy storage and energy upgrade thermochemical solid–gas sorption system for seasonal storage of solar thermal energy.* Energy, 2013. **50**: p. 454-467.

34. Mette, B., et al., *New highly efficient regeneration process for thermochemical energy storage.* Applied Energy, 2013. **109**: p. 352-359.

35. Stitou, D., N. Mazet, and S. Mauran, *Experimental investigation of a solid/gas thermochemical storage process for solar air-conditioning.* Energy, 2012. **41**(1): p. 261-270.

36. Tanguy, G., et al., *Parametric studies of thermochemical processes for seasonal storage.* Energy Procedia, 2012. **30**: p. 388-394.

37. Zondag, H., et al., *Prototype thermochemical heat storage with open reactor system.* Applied Energy, 2013. **109**: p. 360-365.

38. Aydin D, Casey SP, Riffat S. *Numerical Analysis of Solar Assisted Seasonal 'Open' Thermochemical Heat Storage.* International Journal of Low Carbon Technologies, 2015. **10**(2): p. 131-138.

39. Aydin D, Casey SP, Riffat S. *Theoretical analysis of the potential for thermochemical heat storage under Mediterranean climate conditions: Northern Cyprus Case*. Future Cities and Environment, 2015. **1**(2). DOI 10.1186/s40984-015-0003-x.

40. Aydin D, Casey SP, Chen X, Riffat S. *Novel 'open-sorption pipe' reactor for solar thermal energy storage.* Energy Conversion and Management, 2016. **121**: p. 321–334.

41. Casey, S.P., et al., *Salt impregnated desiccant matrices for 'open' thermochemical energy storage—Hygrothermal cyclic behaviour and energetic analysis by physical experimentation.* Energy and Buildings, 2015. **92**(0): p. 128-139.

42. Casey, S.P., et al., *Salt impregnated desiccant matrices for 'open' thermochemical energy storage—Selection, synthesis and characterisation of candidate materials.* Energy and Buildings, 2014. **84**(0): p. 412-425.